Method for Generation of Pendant Drops Through Localized Condensation for Contact

Angle Measurements in Conditions Deviating from Standard Environment

by

Ajay Roopesh Mohan

A Thesis Presented in Partial Fulfillment
of the Requirements for the Degree
Master of Science

Approved November 2015 by the
Graduate Supervisory Committee:

Konrad Rykaczewski, Chair
Robert Wang
Marcus Herrmann

ARIZONA STATE UNIVERSITY

December 2015

ABSTRACT

Contact angle goniometer is one of the most common tools in surfaces science. Since the introduction of this instrument by Fox and Zisman[1] in 1950, dispensing the liquid using a syringe has generated pendant drops. However, using such approach at conditions significantly deviating from standard pressure and temperature would require an elaborate and costly fluidic system. To this end, this thesis work introduces alternative design of a goniometer capable of contact angle measurement at wide pressure and temperature range. In this design, pendant droplets are not dispensed through a pipette but are generated through localized condensation on a tip of a preferentially cooled small metal wire encapsulated within a thick thermal insulator layer. This thesis work covers experimental study of the relation between the geometry of the condensation-based pendant drop generator geometry and subcooling, and growth rate of drops of representative high (water) and low (pentane) surface tension liquids. Several routes that the generated pendant drops can be used to measure static and dynamic contact angles of the two liquids on common substrates well as nanoengineered superhydrophobic and omniphobic surfaces are demonstrated.

DEDICATION

I would like to dedicate this to my parents for their constant love and support that helped me get through tough times at Arizona State University. I would also like to thank my sister for always being there for me and supporting me financially and morally. And finally, I would like to thank all my friends, without whom none of my success would be possible.

ACKNOWLEDGMENTS

I would like to express my deepest appreciation to my committee chair, Dr.Konrad Rykaczewski, for the enthusiasm, advices, valuable comments, constant motivation and the provisions that benefited me in completing this project. Without his guidance and persistent help this thesis wouldn't have been possible.

I would also like to thank my committee members: Dr.Robert Wang and Dr.Marcus Herrmann for their insightful comments and remarks.

I would also like to thank my lab mates in Dr. Rykaczewski's research group: Viraj Damle and Xiaoda Sun for helping me out with my project, giving me useful suggestions that helped me complete the project successfully.

And finally, I would like to thank Ira. A. Fulton School of Engineering at Arizona State University for supporting this research.

TABLE OF CONTENTS

LIST OF TABLES

LIST OF FIGURES

INTRODUCTION

Contact angle goniometer is one of the most common tools in surfaces science. Since the introduction of this instrument by (Fox and Zisman in 1950), pendant drops have been generated by dispensing the liquid using a syringe. However, using such approach at conditions significantly deviating from standard pressure and temperature would require an elaborate and costly fluidic system.. Measurement of surface tension at elevated pressures and low temperatures is possible (Drelich, J.; Fang, C.; White, 2002) but measurement of drop contact angles without complicated and costly cryogenic fluidic system is challenging. Blake et al. (Blake et al. 1971) introduced an alternative simple method that consisted of a hollow stem that was internally cooled via few drops of liquid nitrogen. While effective, this method did not provide any control over temperature of the stem, and with that the drop.

To increase the rate of droplet generation, a simple preferential condensation mechanism is proposed. Specifically, the schematic in Figure 1.1 shows that preferential cooling of a metal tip within the environmental chamber is achieved by encapsulating a thermally conductive metal wire along central axis of a thermally insulating cylinder. When the top of the assembly is cooled, the tip of the thermally conductive wire should cool significantly faster and remain at the desired temperature for much longer than the surface of the thermally insulating block. Preferential condensation onto the thermal conductor tip can be achieved by tuning the temperature of the cooling plate, and with that the exposed metal tip, below the saturation temperature of the vapor. Because of the delayed cooling of the surface of the thermally insulating block, for a period of time condensation should be localized only to the metal tip. A similar preferential

1

condensation approach, albeit on much smaller scale, was successfully implemented by Rykaczewski and Scott (Rykaczewski and Scott, 2011) to image condensation on nano-to-microscale water droplets on superhydrophobic nanostructures within an environmental scanning electron microscope (ESEM). Using this approach, the authors achieved a ~30 s delay between condensation onto a sample mounted to an exposed copper microfinger and surface of surrounding thermally insulating ~0.5 to 1 mm thick cyanoacrylate. In this work, the "macroscale" equivalent of this concept is developed and its use for integration into a contact angle goniometer is demonstrated (see Figure 2.3). First, thermal simulations were used to show that by scaling up the proposed geometry to the millimeter scale, there could be significant increase in preferential cooling time. Second, a prototype device is used to condense pendant drops of a representative high (water) and low (pentane) surface tension liquid on various geometries of the metal wire tip (see Figure 2.1). Several routes of using the generated pendant drops to measure static and dynamic contact angles of the two liquids on common substrates as well as nanoengineered superhydrophobic and omniphobic surfaces.
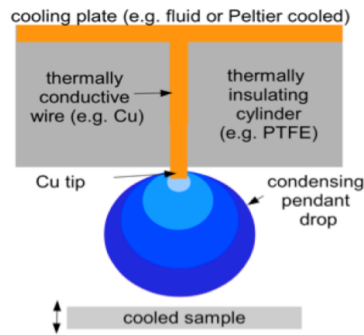
Figure 1.1: Schematic of thermal conductor embedded within thermal insulator block used for generation of pendant drops via preferential condensation

2

BACKGROUND

Condensation basics

The phenomenon of condensation occurs when a saturated vapor comes in contact with a body whose temperature is below the saturation temperature of the vapor. The condensation process starts with heterogeneous nucleation of the liquid at the surface and can proceed in filmwise or dropwise mode, depending on whether or not the condensate wets the surface. If the surface is completely wetted by the vapor, or has a high degree of pinning (large contact angle hysteresis) a continuous condensate film will forms on the interface. This mode of condensation is called filmwise condensation (FWC). Alternatively, if the surface is not wetted by the condensate and has a low contact angle hysteresis, droplets will grow, coalesce, and eventually shed of the surface due to gravitational forces. This mode is referred to as dropwise condensation (DWC). Generally, the dropwise mode is preferred over filmwise mode as the overall heat transfer coefficient in the former mode is 5 to 10 times higher than in the latter.

Condensation rate enhancement via surface engineering

Since the 1930s, hydrophobization of metal surfaces has been known to increase heat transfer during water condensation by up to an order of magnitude (Schmidt et al. 1930) , whereby this surface modification switches the condensation mode from FWC to DWC. Moreover, studies have also shown that further increases in DWC rates can also be achieved by decreasing the threshold radius for gravity-driven droplet shedding (Rose 2002). This can be accomplished through nano-texturing of surfaces to make them superhydrophobic. Anand et al. (Anand et al. 2012) have demonstrated that the water

3

departure diameter also significantly decreased during DWC on nanotextured lubricant impregnated surfaces (LIS). Industrial applications of water DWC promoters in the past have been hindered by their limited longevity. However, durable hydrophobic materials developed recently, including rare earth oxides(Azimi et al. 2013), grafted polymers(Paxson et al. 2014), and the self-healing LIS (Anand et al. 2012, Xiao et al. 2013) are promising candidates for resolving the durability issue.

In recent work, Rykaczewski and co-authors have demonstrated that properly engineered omniphobic surfaces can, in fact, promote DWC and, as shown in Figure 2.1, and can enhance the condensation rate of low surface tension (low-σ) fluids by four to eight-fold (Rykaczewski et al. 2014). The authors also extended and validated DWC heat transfer models (Kim et al. 2011) to predict heat transfer coefficient h for the DWC of low contact angle drops. The model predicts heat transfer through a drop with radius r and contact angle θ (Kim et al. 2011) :

$$q_d = \frac{\Delta T \pi r^2 (1 - \frac{r_c}{r})}{\left(\frac{\delta}{sin^2 \theta k_{coat}} + \frac{r\theta}{4 k_w sin\theta} + \frac{1}{2 h_i (1 - cos\theta)} \right)} \tag{2.1}$$

where ΔT, r_c, h_i, δ, k_{coat}, k_w, and are the surface subcooling, critical nucleation radius, interfacial liquid-vapor heat transfer coefficient, thickness of the coating, and thermal conductivities of the coating and liquid water, respectively. The overall heat transfer rate per unit area for different surface subcooling was obtained by integrating the product of q_d and drop size distribution, $n(r)$, from r_c to the departure radius $r_d = D/2sin\theta$:

$$q'' = \int_{r_c}^{r_d} q_d\, n(r)dr \qquad (2.2)$$

h is obtained by linear fitting of the calculated heat transfer rate per unit area for modeled surface subcooling range.
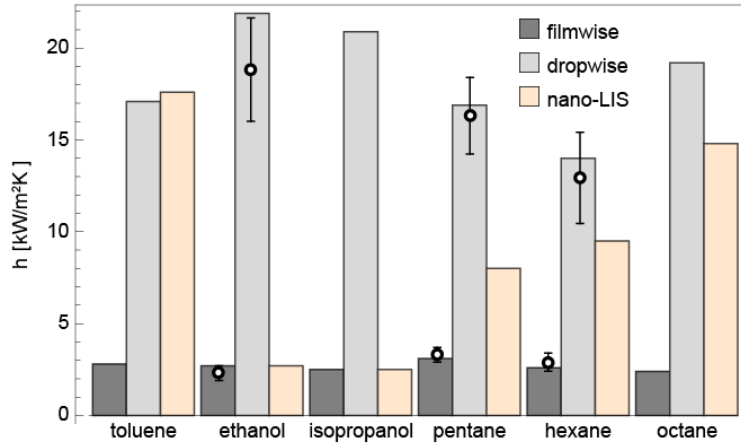
Figure 2.1. Measured and predicted enhancement of heat transfer coefficients (HTC) on omniphobic surfacse. The predicted filmwise HTC was calculated from linear fit to Nusselt model and the predicted dropwise HTC on smooth and Krytox-impregnated nano-textured omniphobic surfaces (nano-LIS) was calculated using Eq. 2.1 with experimentally-determined departing diameters. Experimental heat transfer coefficients measurements are indicated with points (Rykaczewski et al. 2014).

Wetting states and condensation on nanoengineered omniphobic surfaces

"Liquid-phobicity" of a surface can be interpreted as the ease with which a surface sheds-off drops. These characteristics are manifested via the geometry of the drops as they interact with the surface. Drops with diameters below the liquid's capillary length are assumed as spherical caps and are characterized by measuring their contact

5

angles. From a DWC perspective, the contact angles that a drop forms while advancing onto (θ_A) and receding from (θ_R) a surface are of particular importance because they define the departure diameter and with that the DWC heat transfer coefficient (Figure 2.2a) (Rose 2002). In particular, the smaller the difference between θ_A and θ_R, (i.e., contact angle hysteresis (CAH)), the more "liquid-phobic" the surface, and the smaller the drop departure diameter.
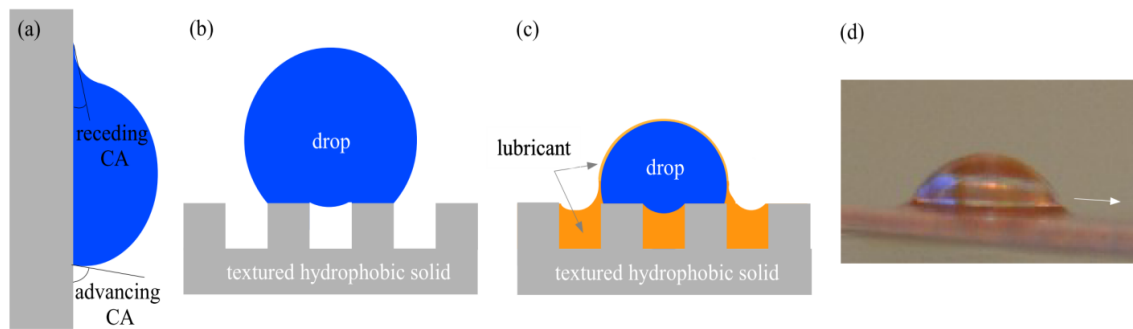
Figure 2.2. Schematic of (a) drop sliding from vertical smooth surface with receding and advancing contact angles (CA) indicated, (b) superhydrophobic surface, (c) lubricant impregnated surface (LIS), and (d) example of a 4 μL drop of ethanol sliding off a LIS at about a 5° tilt with negligible contact angle hysteresis.

Low CAH can be achieved on low surface energy materials with surfaces that are (a) very smooth, (b) nano/microstructured, and (c) nano/microstructured and impregnated with a low surface-energy lubricant (see corresponding schematics in Figure 2.2). An example of the first approach is flat silicon wafer modified with fluorosilane coatings. As long as the spreading coefficient of the liquid (subscript c) on the solid (subscript s) in presence of vapor (subscript v), $S_{cs(v)}$, is negative, a drop with a finite θ will form. The $S_{cs(v)}$ is equal to $\sigma_{sv} - \sigma_{cv} - \sigma_{cl}$, where σ_{ij} corresponds to interfacial tensions between

6

i-j phases. For water ($\sigma_{cv} = 72$ mN/m) deposited or condensing on highly-fluorinated materials such as trichloro(1H,1H,2H,2H-perfluorooctyl)silane ($\sigma_{sv}\sim10$ mN/m), drop formation and shedding can be expected. While a negative $S_{cs(v)}$ is not probable for liquids with σ_{cv} much lower than water, Figure 2.3a shows the DWC of liquids with $\sigma_{cv}\sim15\text{-}30$mN/m on the silaned silicon wafer. Thus, as a rough rule-of-thumb, the DWC of liquids with $\sigma_{cv} > \sigma_{sv}$ could occur on absolutely smooth surfaces. This offers a simplistic argument for first estimate of feasibility of DWC while neglecting σ_{cl}, since these values are often not available in the literature.
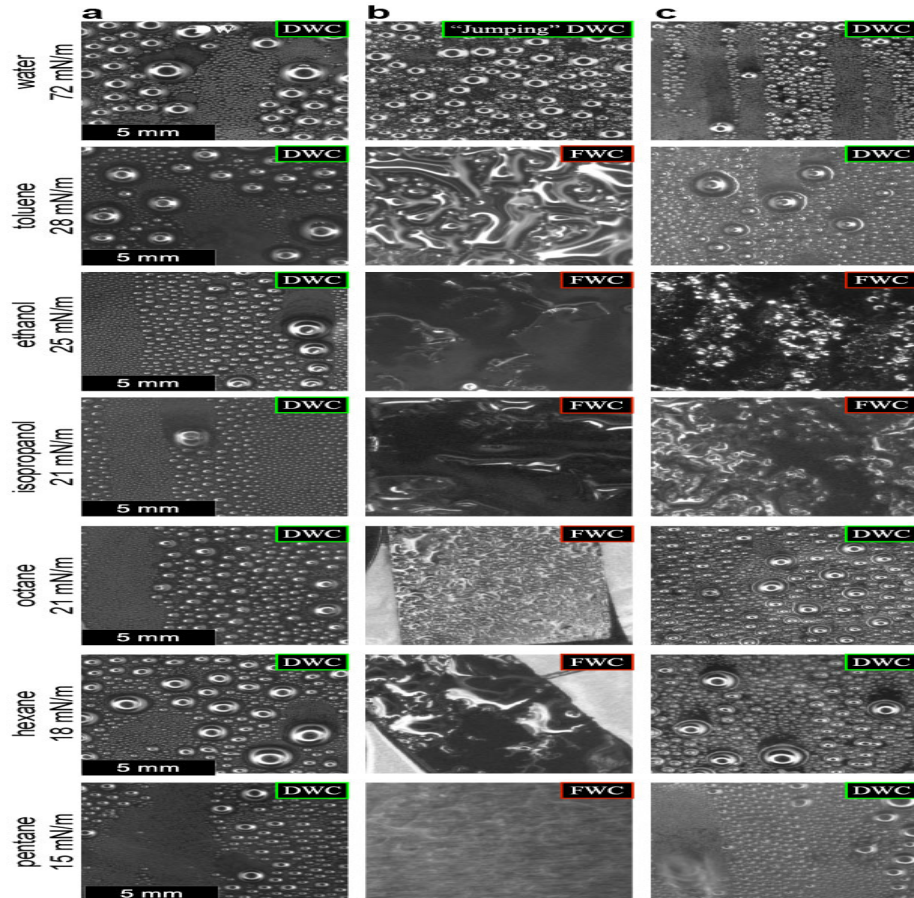
Figure 2.3. Effect of condensate interfacial tension on condensation mode on different

surfaces. Condensation of various low-surface tension fluids on a (a) smooth oleophobic surface, (b) unimpregnated nanotexture, and (c) Krytox-impregnated nanotexture. DWC and FWC stand for dropwise and filmwise condensation, respectively.

The second approach to achieving low CAH relies on surface nano/micro-texturing, which according to Wenzel's equation should amplify the wetting properties (from θ to θ_e):[69,70]

$$\cos\theta_e = R\cos\theta \qquad (2.3)$$

where R is the ratio of true to the apparent/projected surface areas. While for water with $\theta > 90°$ a $\theta_e > 150°$ can be easily achieved, for liquids with low σ_{cv} ($\theta \ll 90°$ on the fluorinated silicon) condensation on hydrophobic nanotextured results in surface flooding (see Figure 2.3b). A similar result was obtained on surfaces with re-entrant geometrical surface features (Rykaczewski et al. 2014), which display robust omniphobic properties for deposited macroscopic drops of low σ_{cv} liquids (Tuteja et al. 2007, Tuteja et al. 2008). This mismatch between wetting observed for deposited and condensed droplets is due to nanodroplets nucleating within the texture.

In the third approach, low CAH of deposited drops of liquids ranging from water to pentane can be achieved by impregnating hydrophobic nanotextured surfaces with a low-surface energy lubricant (see Figure 2.2c-d) (Lafuma et al. 2011, Wong et al. 2011, Anand et al. 2012, Kim et al. 2013, Smith et al. 2013). In addition to immiscibility with the contacting liquids, the other requirement for achieving stable omniphobic LIS characteristics is that the lubricant must impregnate the textured surface (Lafuma et

8

al. 2011, Seiwert et al. 2011, Anand et al. 2012, Smith et al. 2013). This is achieved only if the contact angle that a drop of the lubricant (l) makes on the flat solid (s) in presence of the gas/vapor (v, thus $\theta_{ls(v)}$) is lower than the critical impregnation angle (θ_c) (Lafuma et al. 2011):

$$\theta_{ls(v)} < \theta_c = cos^{-1}\left(\frac{1-\phi}{R-\phi}\right) \qquad (2.5)$$

where   is the ratio of the surface area of the tops over the apparent surface area of the material. However, while the three surface architectures shown in Figure 2.4 satisfy Eq.5, sustained DWC of pentane can be achieved only on the solely nanostructured LIS (Figure 2.4a&d and 2.3c). In contrast, pentane condensation on the micro-structured (Figure 2.4c&f) LIS results in dewetting of the lubricant (Figure 2.4g). Similarly, pentane condensation on the nano/micro-structured (Figure 2.4b&e) LIS, results in quasi-DWC with highly pinned and deformed drops (Figure 4h) (Rykaczewski et al. 2014). Contrasting the SEM images of the lubricated nano-LIS and nano/micro-LIS in Figures 2.4d&e provides a qualitative explanation for the observed "highly pinned DWC" on the hierarchical LIS: the micro-features poking above oil provide pinning points for the drops.

The FWC of isopropanol and ethanol on nano-LIS shown in Figure 2.3c was surprising because these liquids have a higher σ_{cv} than pentane which displayed DWC. This behavior can be explained through LIS wetting states theory developed by Smith et al. (Smith et al. 2013) who have demonstrated that there can be up to 12 thermodynamic configurations of liquid drops on LIS. These states depend on the

9

relation between surface characteristics quantified by R and the interfacial tensions.
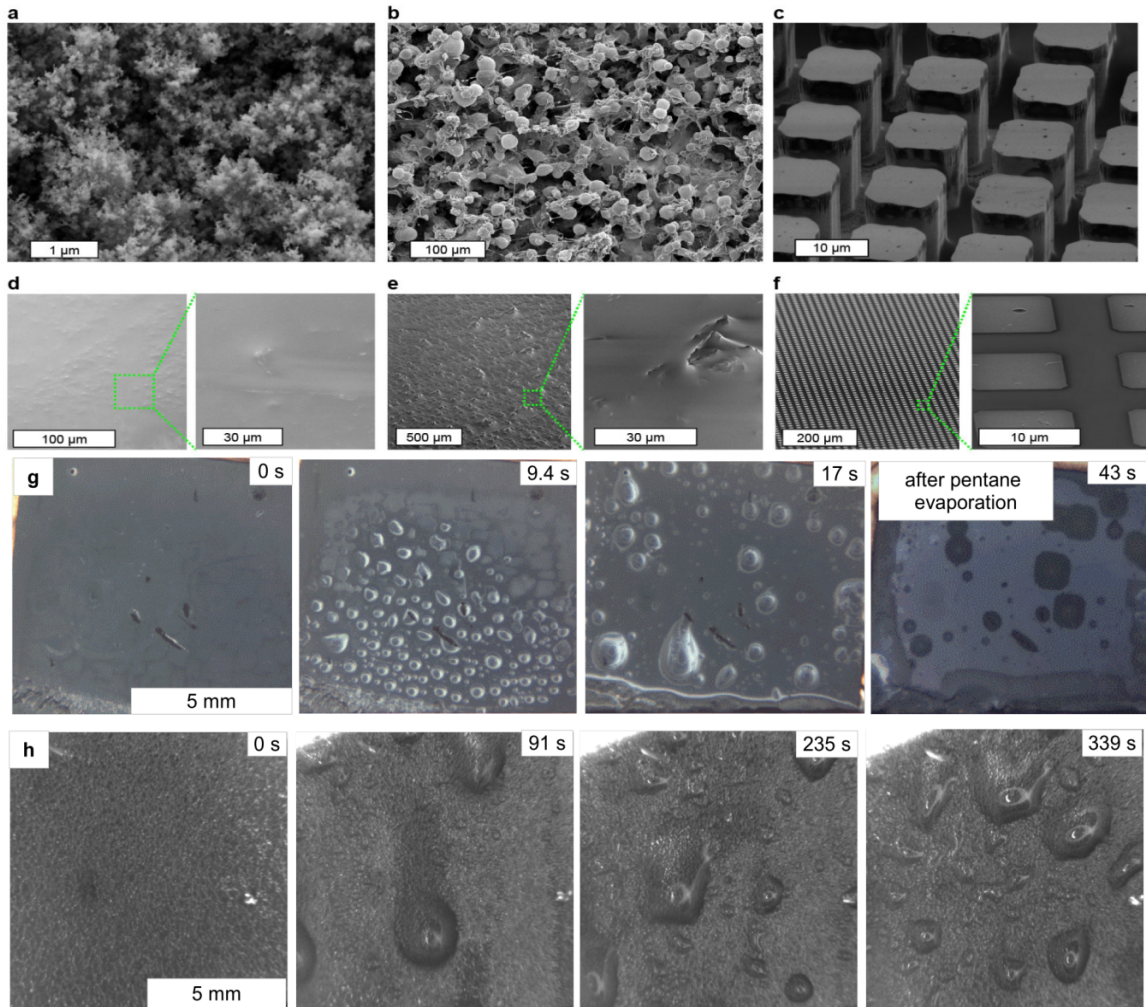
Figure 2.4. (a) to (f) textured surfaces before and after lubricant impregnation: (a) vapor-deposited alumina-silica nanotextured, (b) re-entrant superomniphobic texture, (c) Silicon microposts etched via photolithography, (d) Krytox-impregnated nanotextured, (e) Krytox-impregnated superomniphobic texture, and (f) Krytox-impregnated microposts; (g) impregnated microposts are displaced by condensing pentane, and (h) Krytox-impregnated

Three of these wetting states corresponding to the situation occurring during condensation of the low-σ_{cv} fluids on the nano-LIS and micro-LIS are shown in Figure 2.5. These condition include $\theta_{ls(v)} < \theta_c$ as well negative spreading coefficient of the lubricant on the condensate ($S_{lc(v)}$), which is equal to $\sigma_{cv} - \sigma_{lv} - \sigma_{cl}$. A $S_{lc(v)} > 0$, which occurs during condensation of water on LIS with Krytox, is detrimental to condensation because it causes "cloaking" of the drops by the lubricant. Anand et al.(Anand et al. 2012) have shown that this process can slow down droplet growth as well as deplete the lubricant over prolonged condensation times.
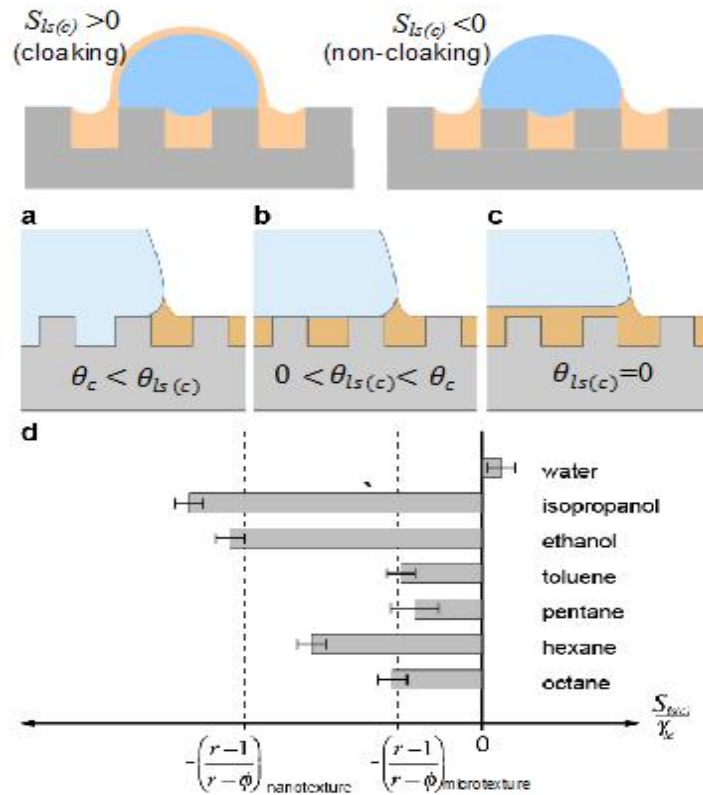
Figure 2.5. Three out of twelve possible thermodynamic states of a liquid droplet

placed on a LIS: (a) impaled that leads to FWC, (b) non-impaled with emergent surface features that promotes DWC, and (c) "floating" state with lubricant encapsulated surface features that promotes DWC and least drop adhesion. The top two schematics show whether or not the droplet gets cloaked by the lubricant, the below states are for $S_{ls(c)}$ <0 (non-cloaking) and $\theta_{ls(v)} < \theta_c$. The possible states depend on how the lubricant wets the texture in the presence of condensate water (horizontal axis) (Smith et al. 2013).

Because of the surface tension being comparable to that of the lubricant ($\sigma_{lv} \sim 17$ mN/m), cloaking of the tested low σ_{cv} fluids was avoided (Rykaczewski et al. 2014). For these conditions, Smith et al.(Smith et al. 2013) have demonstrated that if the spreading coefficient ($S_{ls(c)}$) of the lubricant on the solid in the presence of condensate is greater than zero, i.e., $S_{ls(c)}$ >0, then the condensate drops will float on a thin film of lubricant with virtually no pinning (Figure 2.5c). If $S_{ls(c)}$ <0, then in order to prevent the condensate from displacing the lubricant (Figure 2.5a), the surface lubricant and solid must possess surface tensions in relation to the surface roughness such that:

$$-\left(\frac{R-1}{R-\phi}\right) < \frac{S_{ls(c)}}{\sigma_{lc}} < 0 \tag{6}$$

Figure 2.5d shows that $S_{ls(c)}$ of Krytox in the presence of isopropanol and ethanol is much lower than with pentane or hexane, so the former two liquids act to destabilize the lubricant film and impale the solid texture. In addition, only the spreading coefficient of water on the solid in presence of the condensate is greater than $-(R - 1/R - \phi)$, explaining why the micro-textured LIS de- wet during condensation of the other

12

fluids. These experiments and supporting theory highlight that the wetting states along with the condensation modes are highly dependent on the spreading coefficients of the lubricant on the solid surface, not only in the presence of vapor, but also in the presence of the condensate. Eq. 6 can also be expressed in terms of the contact angle that the drop of the lubricant makes with the solid in presence of the condensate ($\theta_{ls(c)}$):

$$\frac{S_{ls(c)}}{\sigma_{lc}} = \frac{\sigma_{cv} - \sigma_{lv} - \sigma_{cl}}{\sigma_{lc}} = \frac{\sigma_{cl}(\cos\theta_{ls(c)} - 1)}{\sigma_{lc}} = \cos\theta_{ls(c)} - 1 \ \& \ 1 - \left(\frac{R-1}{R-\phi}\right) = \cos\theta_c \rightarrow \theta_{ls(c)} < \theta_c \quad (7)$$

EXPERIMENTAL METHODS

Goniometer Prototype

To demonstrate the preferential condensation mechanisms and its integration into a goniometer, a copper wire was embedded along the central axis of a Polytetrafluoroethylene (PTFE from McMaster-Carr) cylinder with height and diameter of 6.5 cm and 4.1275 cm, respectively. The bottom surface of the PTFE cylinder was machined with a conical taper of ~5° to facilitate visual access to the center of the bottom surface that is exposed to the vapor (see Figure 3.1). The diameter of the copper wire was selected to be smaller than the capillary length of the tested liquid, $l_c = \sqrt{\sigma/\rho g}$ (where g, σ, and g are the gravitational constant (9.8 m/s^2) and the liquid's surface tension and density).

Sessile drops whose largest dimension (base diameter for drops with static contact angle, θ_s, less than or equal to 90°) is smaller than the capillary length will not be distorted by gravity and will take on a spherical cap shape (i.e. their shape can be characterized by diameter and contact angle). Thus, the condensed pendant drops should also have diameters smaller than l_c. Wires with diameters of ~1.6 mm and ~1.0 mm were used for measurements with water and pentane, which have l_c of ~2.7 mm and ~1.6 mm, respectively. The wire was tightly fitted into a hole drilled into the PTFE cylinder. The thermal contact resistance between the wire and the cooling block reduced with thin layer of thermal grease (Thermaltake TG-2). Besides large mismatch in thermal conductivities (~400 W/mK vs. ~0.25 W/mK), copper and PTFE also have significantly different surface energies (i.e. low and high contact angles of water). This mismatch in

14

wetting properties should provide additional enhancement in the localized condensation mechanisms due to inhibition of drop nucleation by less wetting surfaces (Israelachvili 2011).
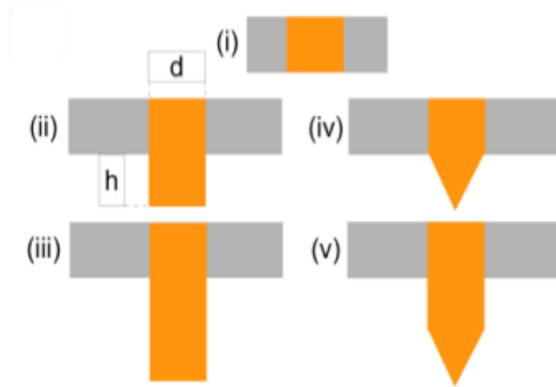
Figure 3.1: Various metal tip geometries studied: (i) flush, (ii) short extended cylinder, (iii) long extended cylinder), (iv) short cone, and (v) long extended cone.

Preferential condensation on five geometries of the exposed metal wire tip shown in Figure 1b was studied. The five types were: (i) flush, (ii) short extended cylinder, (iii) long extended cylinder, (iv) short cone, and (v) long extended cone. The short and extended tips had heights of ~1 mm and ~2 mm outside of the PTFE surface. The conical 60° taper on the copper wire was fabricated manually using a metal polisher (XP8 polisher from Ted Pella Inc. with 1200 grit sand paper).
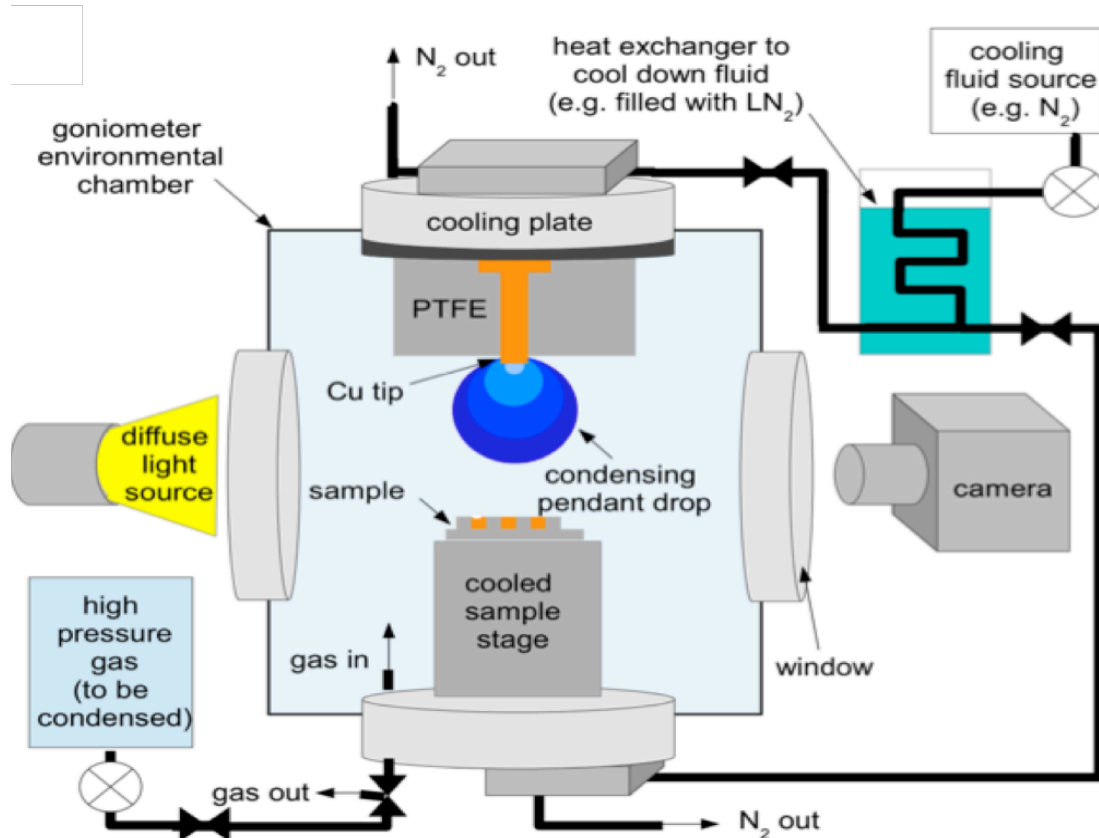
Figure 3.2: Example way to integrating the preferential condensation pendant drop generator into a contact angle goniometer setup with an environmental chamber.

Figure 3.2 shows a general route that the copper-PTFE block assembly can be integrated into a goniometer consisting of an environmental chamber with axially facing viewports: one for optical access for camera (USB CCD camera DFK23U618 from ImagingSource with high magnification Navitar 6232A lens) and one for diffusive back light illumination (MH 100 from Fiber-lite). In the general case, the environmental chamber can be designed to withstand desired pressure range, while the sample and top of the PTFE block with copper wire can be cooled convectively through flow of a cooling fluid.

16

If cryogenic temperatures are required, this flxuid could be dry nitrogen gas cooled to cryogenic temperatures by passing through a heat exchanger filled with liquid nitrogen. To demonstrate the general principle of the goniometer, the described worked focused on preferential condensation of water (purified to 18.2 MΩcm using Nanopure Diamond system from Barnstead) and pentane (99%, Sigma-Aldrich). Since these liquids can be easily condensed at near standard pressure and temperature conditions, a chilled water-cooled Peltier element (2.5 cm by 2.5 cm ATE1-49 from Analog Technologies) was used to cool the top of the PTFE-Cu block. The Peltier element was secured to the outside of top an aluminum port of the cross-pipe fitting vacuum chamber used in Rykaczewski et al. (Rykaczewski et al. 2014). The only modifications to the environmental chamber from that work were addition of the PTFE-Cu block, a bottom venting port, and a small beaker for storing the source liquid water or pentane. Temperatures at different locations in the environmental chamber were measured using K-type thermocouples attached to DAQ system (Omega 8/16-Channel Thermocouple/Voltage Input USB Data Acquisition Module). The temperature of the exposed copper wire tip was not measured directly as presence of thermocouple would alter condensation dynamics. Control experiments were carried out to characterize the difference between the temperature of exposed part of the wire and an easier to access location 3 cm higher along the wire. It was observed that both the temperatures were within ~1 to 2 K of each other from shortly after start until the end of the experiment. Hence, the four K-type thermocouples locations were set to: (1) in between the peltier element and the cooling plate, (2) junction between the environmental chamber wall and the copper rod, (3) along the wire 3 cm above the exposed tip, and (4) within

17

the fluid filling the environmental chamber. To minimize effects of non-condensable gases, a mostly vapor environment was created by decreasing the gauge pressure within the chamber with liquid-filled beaker to below 3.3 kPa (1 inHg) using a vacuum pump (RX5 from Edwards). Since the pressure was decreased to or below the vapor pressure of the two selected liquids ($P_{sat} \sim 50$ kPa for pentane and ~2.3 kPa for water at 293 K), the chamber was filled with nearly pure vapor through forced evaporation of the liquid. The complete setup is illustrated in Figure 3.3 below.
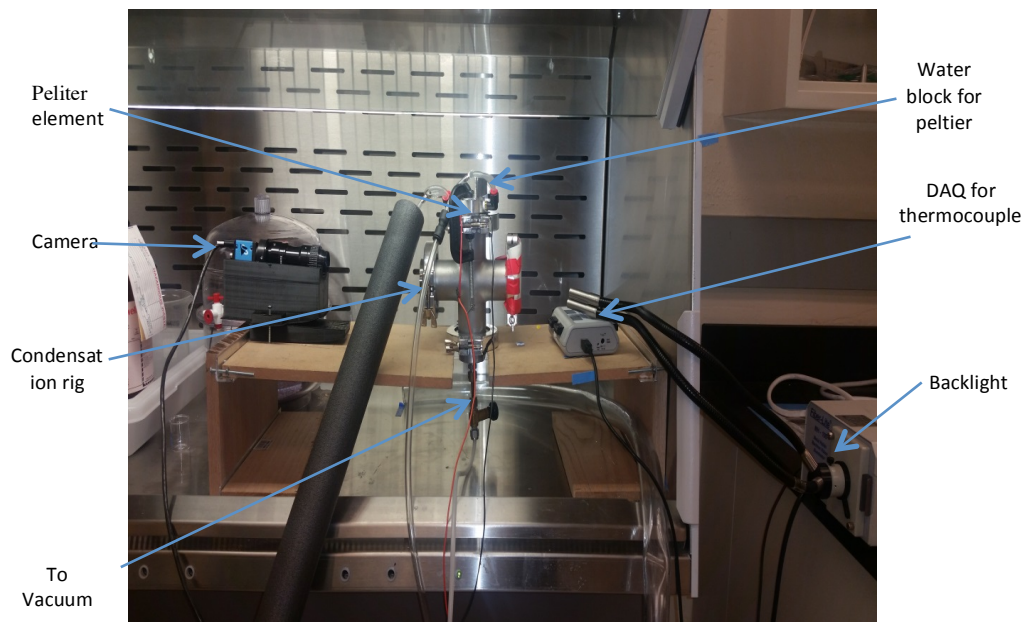
Figure 3.3: Complete experimental setup of the condensation based goniometer

Surface Fabrication Procedure

The contact angles of the different fluids on bare and PTFE modified silicon, mirror polished copper, polymeric superhydrophobic coating, and omniphobic lubricant impregnated surface (LIS) were measured. About 1 cm by 1 cm silicon wafer pieces (University Wafers) were washed using water and ethanol. Prior to any surface modification, the wafer was also cleaned using oxygen plasma in a plasma reactor

(Blue Lantern from Integrated Surface Technologies) for 1 min at pressure of 250 mTorr and power of 150 W. PTFE precursor solution (AF1600, DuPont) was diluted in FC-40 (Sigma Aldrich) in the ratio 1:4.25 by mass. The solution was mixed in ultrasonicator for 10 s and heated at 75 °C for a few seconds. Subsequently, the mixture was spin-coated on cleaned silicon substrate at 4500 ±60 RPM for 1 min and thermally cured on the hotplate at 120°C for 1 h. ~2.5 cm by ~2.5 cm pieces of copper (McMaster Carr) were mirror polished (XP-8 polisher from Ted Pella Inc.) using three polishing steps with 600, 1200, and 1800 grit sandpaper. Some of these copper samples were modified using commercial superhydrophobic coating (Hydrobead). The coating was allowed to dry in air for 30 min. The LIS coating consisted of a copper substrate with a superhydrophobic ceramic nanoparticle coating (Repellix from Integrated Surface Technologies Inc.) infused with perfluorinated Krytox vacuum pump oil. Further details for the Repellix and LIS fabrication are described elsewhere (Chinn et al. 2010, Rykaczewski et al. 2011, Rykaczewski et al. 2013).

Contact angle measurement and quantification

The substrate on which the contact angle of the fluid is to be measured was introduced into the goniometer device and placed on a stage at a distance of ~5 mm from the tip of the extended surface. Once the pendant droplet is formed inside the chamber, short manual tap on the top of the outside of the goniometer device was used to detach the drop. The image of the drop was captured using camera (USB CCD camera DFK23U618 from Imaging Source with high magnification Navitar 6232A lens) and the static contact angle was measured using ImageJ software. The measured values were compared with the static angles measured using a traditional goniometer.

19

RESULTS AND DISCUSSION

Preferential Cooling Analysis

Finite element analysis was used to quantify the degree of preferential cooling of the metal tip as compared to the PTFE block surface. In particular Comsol Multiphysics was used to simulate transient heat conduction within the composite cylinder with initially uniform temperature of 293K. At the beginning of the simulation the top surface of the 1 mm thick cooling plate is subjected to a step 5 K or 10 K decrease in temperature, while the bottom and sides of the block are heated through natural convection (environment temperature of 293 K and a heat transfer coefficient of 5 W/mK (Incropera et al. 2002)). The plots in Figure 4.1 (a) show 2D temperature distributions at 60 s, 1200 s, and 1800 s into the cooling process with a 10 K temperature decrease at the top of the cooling plate. The plots in Figure 4.1 (b) show transient temperatures at points A (1.6 mm diameter copper wire-PTFE interface at the exposed surface) and B (1 mm away from point A along radial direction) for 5 K and 10 K temperature decrease. In both cases temperature of the copper tip (being lowest at point A) decreases within ~60 s to 1 to 2 K of the temperature of the top of the cooling plate. In turn, the temperature decrease at point B is much slower. Furthermore, even after 1 h of cooling there is a 1 K and 2 K temperature difference between points A and B for the 5 K and 10 K initial temperature decrease of the cooling plate. These simulations indicate that with the proposed scheme, preferential cooling of the copper tip of several degrees Kelvin for at least ~30 to 60 minutes should be achievable. The results also indicate that the temperature of the cooling plate could be tuned so that the saturation temperature falls between that of the tip and the

20

surrounding PTFE surface.

This procedure should yield preferential condensation just onto the tip of the wire. Also, it is noted that onset of the phase change process will release substantial quantity of heat into the copper wire. Since the performed simple simulations are intended to be only qualitative guides, condensation is not incorporated into the simulations. In agreement with our control experiments described in previous section, the simulations indicate a minor temperature difference between the tip and first 2 to 3 cm of the copper wire.
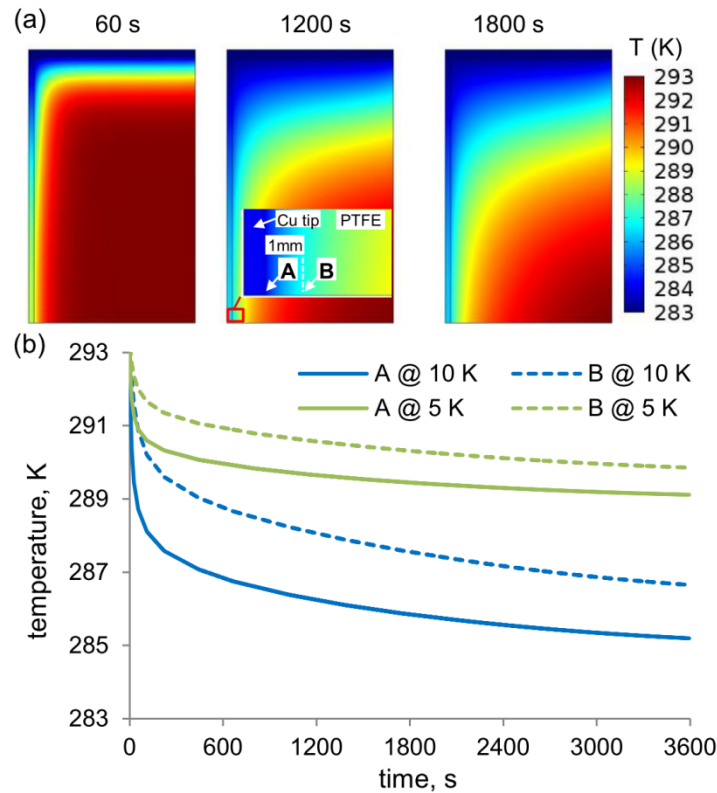
Figure 4.1. Transient heat conduction simulation of composite copper-PTFE cylinder: (a) 2D temperature maps at 60 s, 1200 s, and 1800 s after temperature of the top of the block is decreased by 10 K and (b) transient temperatures at points A and B indicated in plot in (a) for 5 K and 10 K temperature 21 decrease at the top of the block.

Water and pentane pendant drop generation via localized condensation and static contact angle measurement
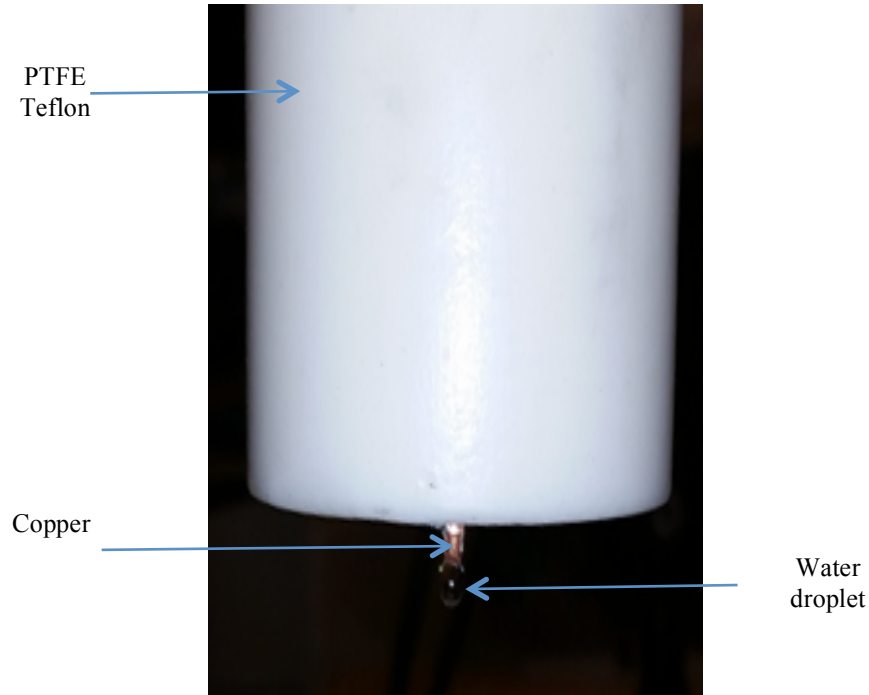
Figure 4.2: Inside the environmental chamber. Condensation on the extended surface

The images in Figure 4.2 and 4.3 a & b clearly show that by cooling top of the plate, achieved preferential condensation of both water and pentane onto the exposed tip of the wire. The top plate was cooled to ~275 K leading to cooling of the metal wire to ~277 K. In both the case of water and pentane the chamber temperature was ~281 K, leading to subcooling of the exposed tip of ~14 K (assuming 100% vapor in the chamber). In agreement with the above simulations, no major signs of condensation onto the neighboring PTFE block surface during the experiments was observed. Because of its much higher vapor pressure (~ 50 kPa vs. ~2.3 kPa at 293 K), drops of pentane formed faster than drops of water. In particular, the first drops of water were fully formed

within 45 to 60 min, while first drops of pentane fully developed within 15 to 20 min after start of cooling.

The geometry of the condensed pendant drops strongly dependent on the geometry of the exposed tip and on the properties of the liquid itself. The water condensation proceeded through condensation of numerous microdroplets that within a few minutes coalesced to form a single larger drop or sagging film (i.e. typical dropwise to filmwise condensation transition) (Rose 2002, Beysens 2006). In all cases water was mostly confined to the hydrophilic metal surface and did not spread onto surrounding highly hydrophobic PTFE (Figure 4.3 (a) and (b)). It was found that condensation onto the extended cylinder was more consistent and repeatable than on the cone ended wires. In particular, water always accumulated on the bottom of the cylinders. After reaching this size, the lateral dimension of the water drops was confined to the diameter of the cylinders. Subsequently the water drops grew mostly by increasing their vertical dimension. A larger volume of water appeared to condense onto the cone ended wires, however, the resulting drop geometry was unpredictable. In particular, the images in Figure 4.3 (a) show that a drop suspended from the side of the cone tip. This behavior was undesirable , since in this case geometry of the exposed wire tip cannot be used to dictate the shape and volume of the drop. As shown in plot in Figure 4.4, the height of the copper tip did not have a major impact on the drop geometry (on longer tips drop could be stretched more in vertical direction).

In contrast to water drops, it was found that pentane drops could easily spread onto PTFE surrounding the copper tip (see Figure 4.3 c). The pendant drop spreading was highly undesirable as it "flattened" the drop, making it significantly more difficult to

23

remove. It was found that the drop spreading behavior did not occur on the extended cylinder shaped wires (see Figure 4.3d). In this case a substantial amount of liquid was present on the entire surface of the cylinder. Pentane condensation proceeded in filmwise mode with gravity causing draining to and accumulation of the liquid in drop-like reservoir at the bottom of the tip. 20 minutes after cooling of the top plate, the first pentane pendant drop naturally shedded due to gravity. Subsequent pentane drops formed and shedded every 3 minutes. This observation corroborates simulations results and indicates about a 10 to 15 minutes initial cooling period required to achieve near steady state temperature (few degrees above the cooling plate temperature).
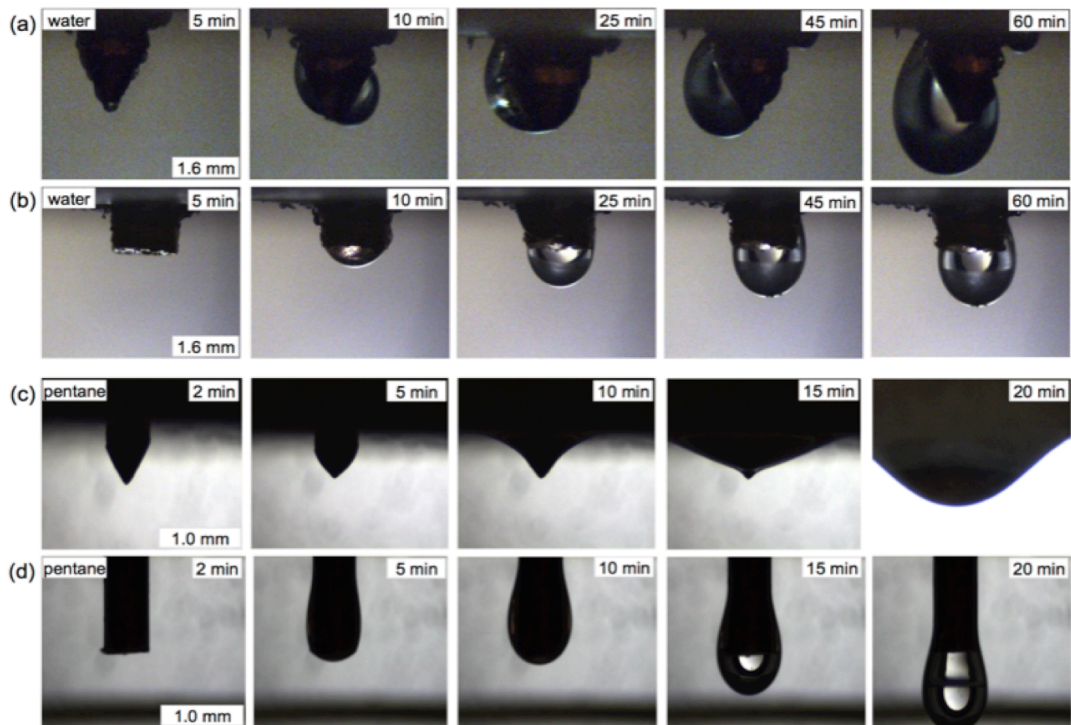

Figure 4.3. Condensation of water (a,b) and pentane (c, d) pendant drops on (a, c) cone-ended and (b, d) cylinder ended preferentially cooled copper wire tips emerging out of a PTFE block.
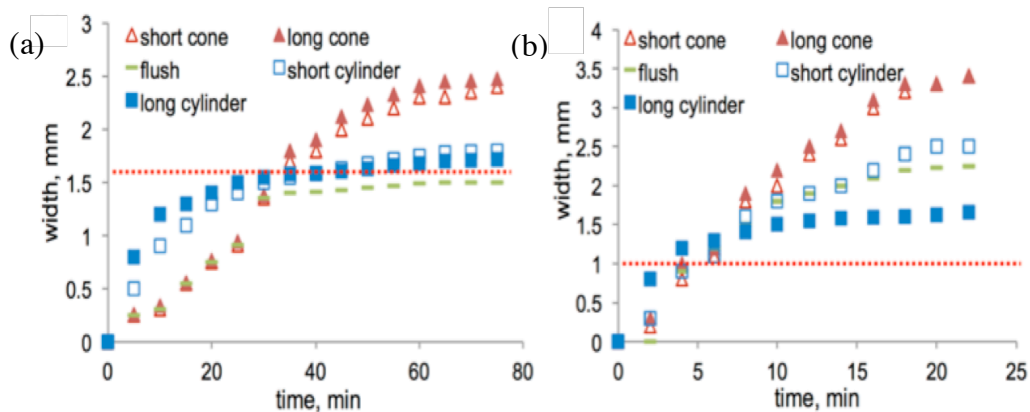
Figure 4.4. Plot of the width of the condensing pendant drops on different wire tip shapes as a function of time for (a) water and (b) pentane condensation experiments; the red dashed lines show the width of the base of the copper wire.

All condensed pendant drops that did not spread onto the PTFE surface could be detached from the wire tip using a short manual tap on the top of the outside of the goniometer device. This fact was used to demonstrate one route that pendant drops generated through localized condensation could be used to measure static contact angles. In particular, prior to start of the condensation experiments different substrates were placed ~5 mm below the tip. After detaching drops with a tap, static contact angles were measured from images of drops that landed onto these substrates. The static contact angles of water measured using the traditional goniometer and this new method on silicon, copper, PTFE film on silicon, and the superhydrophobic coating were 61.2° ± 3.1 vs. 57.8° ± 2.9, 85.2° ± 2.3 vs. 82.6° ± 1.8, 108.5° ± 1.9 vs. 104.5° ± 2.5, and 153.6° ± 2.8 vs. 150.2° ± 2.3, respectively. In turn the corresponding static contact angles for pentane drops were 13.2° ± 1.6 vs. 12.9° ± 1.2, 15.1° ± 1.8 vs. 14.7° ± 0.9, 18.6° ± 1.3 vs. 18.1° ± 0.8, and 27.2° ± 1.6 vs. 26.5° ± 0.9 respectively. The values measured

using the introduced method were typically a few degrees lower than those measured using the outside goniometer. This is likely due to spreading and recoiling dynamics during drop impact or thermal effects (the substrates were not cooled in our prototype goniometer so some evaporation might be occurring)

Dynamic contact angle measurement

The contact angle that a liquid makes advancing onto (θ_A) and receding from (θ_R) a surface are a better measure of droplet adhesion to the surface than static contact angle. The schematic in Figure 4.5a shows that these values are typically quantified from images of a drop that is expanding over and receding from a surface due to liquid addition and subtraction via a syringe, respectively. This method is referred to here as liquid volume variation (VV) method. In general two alternatives to the VV method could be employed for measurement of dynamic contact angles when the pendant drop is generated via condensation (i.e. no syringe). First, placing of the substrate in proximity to the exposed metal tip could allow for observation of expansion and receding of drop in contact in the substrate via additional condensation and evaporation. However, in this case motion of the triple phase line (i.e. contact angle values) might be altered by coalescence with secondary nucleating drops on the surface. A second alternative method is to vary the position of the sample while maintaining volume of the drop constant. Specifically, the schematic in Figure 4.5b shows that advancing contact angle is measured as the sample is pressed against the drop while the receding contact angle is measured as the sample is being lowered. Doudrick et al. (Doudrick et al. 2014) recently used this method, that is referred to as sample height variation (HV), to measure dynamic contact angles of oxide- shell covered GaInSn liquid metal. The

authors also performed control experiments to show that dynamic contact angles of water on PTFE coated silicon wafer measured VV and HV methods did not differ. The HV method was adapted to measure dynamic contact angles of pendant drops hanging from a solid copper tip. For simplicity, contact angles of liquid drops manually suspended from a metal tip, not condensed within the environmental chamber, were measured. Figure 4.5c shows example images of dynamic contact angle measurement for water on PTFE covered silicon wafer using the HV method. This approach was used to quantify advancing and receding contact angles of water and tetradecane on polished copper, cleaned silicon wafer, PTFE coated silicon wafer, as well as SHS and LIS (see experimental section for fabrication details). Low vapor pressure tetradecane was used instead of fast-evaporating pentane to facilitate the experiments in room environment. The values of the dynamic contact angles and their difference (i.e. contact angle hysteresis) presented in Table 3.1 show that the VV and HV methods yielded practically same results in all the tested cases.
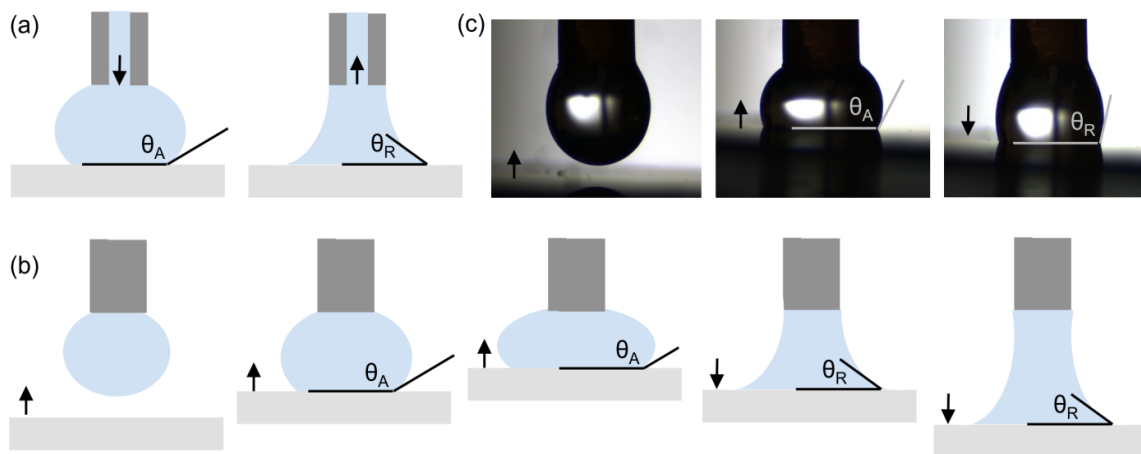

Figure 4.5. Schematic representing measurement of advancing and receding contact angles using (a) standard liquid volume variation method and (b) proposed sample

height variation method, and (c) example images showing silicon wafer with PTFE coating prior to contact, being pushed against and retracted away from a water drop attached to a copper wire tip.

Table 3.1: Summarizes the results of dynamic contact angle measurements (advancing angle, θ_A, receding angle, θ_R and contact angle hysteresis, $\Delta\theta$) using the Height Variation and Volume Variation method on a hydrophilic and a hydrophobic surface

Measurement method	Silicon wafer			Repellix +Krytox oil (LIS)		
	θ_A	θ_R	$\Delta\theta$	θ_A	θ_R	$\Delta\theta$
VV water	61.6 ± 1.8	46.8 ± 2.2	11.5 ± 2.7	134.2 ± 0.7	130.7 ± 1.1	3.5 ± 1.4
HV water	59.7 ± 2.6	44.1 ± 2.3	10.7 ± 3.1	132.7 ± 1.9	127.6 ± 1.4	5.1 ± 1.1
VV tetradecane	12.8 ± 1.2	10.1 ± 0.8	2.7 ± 1.4	63.7 ± 0.8	60.6 ± 0.9	3.1 ± 1.7
HV tetradecane	14.3 ± 1.3	11.4 ± 1.5	2.9 ± 1.6	64.3 ± 1.1	60.7 ± 0.8	3.6 ± 1.3
VV ethanol	14.9 ± 2.2	11.7 ± 1.8	3.2 ± 1.3	63.4 ± 0.9	59.2 ± 1.4	4.2 ± 1.8
HV ethanol	16.1 ± 1.9	13.3 ± 1.7	2.8 ± 1.6	64.7 ± 0.7	61.2 ± 1.2	3.5 ± 1.1

CONCLUSIONS

This thesis demonstrated a new method for generating pendant drops through preferential condensation onto an exposed tip of a copper wire embedded along central axis of a much larger PTFE cylinder. The large difference between thermal conductivities of the two materials enables preferential cooling of the entire copper wire triggered by cooling of top of the block-wire assembly. It was shown that pendant drops of water and pentane can be repeatedly condensed onto ~2 mm long extended cylinder-shaped tips. These drops can be easily detached from the wire using a single tap on top of the environmental chamber and used to measure static contact angles on substrates placed ~5 mm below the metal tip. It was also shown that pendant drops suspended from a tip of a cylindrical wire could be used to measure dynamic contact angles using the sample height variation method. In this approach, the position of the substrate rather than the volume of the drop was varied to observe liquid spreading and retracting from the surface. Thus, only incorporation of a linear actuator into an environmental chamber with the wire-PTFE block assembly is required to measurement of both static and dynamic contact angles using our goniometer design. Consequently, the introduced goniometer design provides a simple way to measure surface wetting properties at any conditions that condensation is possible.

REFERENCES

Fox, H. W.; Zisman, W. A. The spreading of liquids on low energy surfaces. I. polytetrafluoroethylene. J. Colloid Sci. 1950, 5, 514-531.

Drelich, J.; Fang, C.; White, C. Measurement of interfacial tension in fluid-fluid systems. Encyclopedia of Surface and Colloid Science 2002, 3152-3166.

Millette, J. P.; Scott, D. S.; Reilly, I. G.; Majerski, P.; Piskorz, J.; Radlein, D.; Debruijn, T. J. W. An apparatus for the measurement of surface tensions at high pressures and temperatures. The Canadian Journal of Chemical Engineering 2002, 80, 126-134.

Rykaczewski, K.; Scott, J. H. J. Methodology for imaging nano-to-microscale water condensation dynamics on complex nanostructures. ACS Nano 2011, 5, 5926-5968.

Israelachvili, J. N. Intermolecular and Surface Forces. 3rd ed.; Elsevier: San Diego, 2011.

Rykaczewski, K.; Paxson, A. T.; Staymates, M.; Walker, M. L.; Sun, X.; Anand, S.; Srinivasan, S.; McKinley, G. H.; Chinn, J.; Scott, J. H. J.; Varanasi, K. K. Dropwise Condensation of Low Surface Tension Fluids on Omniphobic Surfaces. Sci. Rep. 2014, 4, 4158.

Rykaczewski, K.; Chinn, J.; Walker, M. L.; Scott, J. H. J.; Chinn, A.; Jones, W. Dynamics of Nanoparticle Self Assembly into Superhydrophobic Liquid Marbles during Water Condensation. ACS Nano 2011, 5, 9746-9754.

Chinn, J.; Helmrich, F.; Guenther, R.; Wiltse, M.; Hurst, K.; Ashurst, R. W. Durable Super-Hydrophobic Nano-Composite Films. In NSTI-Nanotech 2010, 2010; Vol. 1.

Rykaczewski, K.; Anand, S.; Subramanyam, S. B.; Varanasi, K. K. Mechanism of Frost Formation on Lubricant Impregnated Surfaces. Langmuir 2013, 29, 5230-5238.

Incropera, F. P.; DeWitt, D. P. Fundamentals of Heat and Mass Transfer. 5th ed.; John Wiley & Sons: Hoboken, NJ, 2002.

Beysens, D. Dew nucleation and growth. Comp. Rend. Phys. 2006, 7, 1082-1100.
Rose, J. W. Dropwise condensation theory and experiment: a review. Proc. Inst. Mech. Eng. A 2002, 216, 115-128.

Doudrick, K.; Liu, S.; Klein, K. L.; Mutunga, E. M.; Varanasi, K. K.; Rykaczewski, K. Different Shades of Oxide: from Nanoscale Wetting to Imprinting of Gallium-based Liquid Metals. Langmuir 2014, 30, 6867-6877.

Anand, S., A. T. Paxson, R. Dhiman, J. D. Smith and K. K. Varanasi (2012). "Enhanced Condensation on Lubricant-Impregnated Nanotextured Surfaces." ACS Nano 6(11): 10122-10129.

Azimi, G., R. Dhiman, H. M. Kwon, A. T. Paxson and K. K. Varanasi (2013). "Hydrophobicity of rare-earth oxide ceramics." Nature Materials 12: 315-320.

Beysens, D. (2006). "Dew nucleation and growth." Comptes Rendus Physique 7(9-10): 1082-1100.

Blake, T., J. Cayias, W. Wade and J. Zerdecki (1971). "Adsorption on flat surfaces. II. Low-energy surfaces." Journal of Colloid and Interface Science 37(4): 678-685.

Incropera, F. P. and D. P. DeWitt (2002). Fundamentals of Heat and Mass Transfer. Hoboken, NJ, John Wiley & Sons.

Kim, P., M. J. Kreder, J. Alvarenga and J. Aizenberg (2013). "Hierarchical or Not? Effect of the Length Scale and Hierarchy of the Surface Roughness on Omniphobicity of Lubricant-Infused Substrates." Nano Letters 13(4): 1793-1799.

Kim, S. and K. J. Kim (2011). "Dropwise Condensation Modeling Suitable for Superhydrophobic Surfaces." Journal of Heat Transfer 133(8): 081502.
Lafuma, A. and D. Quéré (2011). "Slippery pre-suffused surfaces." EPL (Europhysics Letters) 96(5): 56001.

Paxson, A. T., J. L. Yague, K. K. Gleason and K. K. Varanasi (2014). "Stable Dropwise Condensatin for Enhancing Heat Transfer via the Initiated Chemical Vapor Deposition (iCVD) of Grafter Polymer Films." 31 Advanced Materials 26(3): 418–423.
Rose, J. W. (2002). "Dropwise condensation   theory and experiment: a review."

Proceedings of the Institution of Mechanical Engineers Part a-Journal of Power and Energy 216(A2): 115-128.

Rykaczewski, K., S. Anand, S. B. Subramanyam and K. K. Varanasi (2013). "Mechanism of Frost Formation on Lubricant Impregnated Surfaces." Langmuir 29(17): 5230-5238.

Rykaczewski, K., J. Chinn, M. L. Walker, J. H. J. Scott, A. Chinn and W. Jones (2011). "Dynamics of Nanoparticle Self Assembly into Superhydrophobic Liquid Marbles during Water Condensation." ACS Nano 5(12): 9746-9754.

Rykaczewski, K., A. T. Paxson, M. Staymates, M. L. Walker, X. Sun, S. Anand, S. Srinivasan, G. H. McKinley, J. Chinn, J. H. J. Scott and K. K. Varanasi (2014). "Dropwise Condensation of Low Surface Tension Fluids on Omniphobic Surfaces." Scientific reports 4: 4158.

Schmidt, E., W. Schurig and W. Sellschopp (1930). "Versuche über die Kondensation von Wasserdampf in Film- und Tropfenform." Forschung im Ingenieurwesen 1(2): 53-63.

Seiwert, J., C. Clanet and D. Quéré (2011). "Coating of a Textured Solid." Journal of Fluid Mechanics 669: 55-63.

Smith, J. D., R. Dhiman, S. Anand, E. Reza-Garduno, R. E. Cohen, G. H. McKinley and K. K. Varanasi (2013). "Droplet mobility on lubricant-impregnated surfaces." Soft Matter 9: 1772-1780.

Tuteja, A., W. Choi, M. Ma, J. M. Mabry, S. A. Mazzella, G. C. Rutledge, G. H. McKinley and R. E. Cohen (2007). "Designing Superoleophobic Surfaces." Science 318(5856): 1618-1622.

Tuteja, A., W. Choi, J. M. Mabry, G. H. McKinley and R. E. Cohen (2008). "Robust omniphobic surfaces." Proceedings of the National Academy of Sciences: 18200–1820

Wsong, T.-S., S. H. Kang, S. K. Y. Tang, E. J. Smythe, B. D. Hatton, A. Grinthal and J. Aizenberg (2011). "Bioinspired self-repairing slippery surfaces with pressure-stable omniphobicity." Nature 477(7365): 443-447.

Xiao, R., N. Miljkovic, R. Enright and E. N. Wang (2013). "Immersion Condensation on Oil-Infused Heterogeneous Surfaces for Enhanced Heat Transfer." Scientific Reports 3: 1988.